EXCITATION OF SPECIES IN AN EXPANDED ARGON MICROWAVE PLASMA AT ATMOSPHERIC PRESSURE

M. C. García[1], M. Varo and P. Martínez

Departamento de Física Aplicada, Edificio C-2. Campus Universitario de Rabanales. Universidad de Córdoba. E-14071 Córdoba, Spain, Phone: 34 957212633

[1]*Author for correspondence, e-mail: fa1gamam@uco.es*

ABSTRACT.

The excitation capability of an argon microwave plasma flame expanded at atmospheric pressure has been studied. For this purpose, argon with different proportions of nitrogen was introduced at the end of the expanded flame, where the population densities of the atomic argon levels were still high enough. Optical emission spectra allowed the identification of different excited species in the plasma. When argon containing nitrogen was added at the end of the plasma flame, all argon lines emitted in this region were highly quenched, emission due to species containing nitrogen (NH, CN) was enhanced and a noticeable increase in the emission of N_2 ($C^3\Pi_u - B^3\Pi_g$) was observed. On the contrary, the weak emission of N_2^+($B^2\Sigma^+_u - X^2\Sigma^+_g$) was scarcely affected. According to these results it is possible to conclude that metastable argon atoms from the expanded flame are the main energy carriers when generating N_2 reactive species in this plasma zone.

KEY WORDS: High frequency plasma, microwave plasma, atmospheric pressure, optical emission spectra

1. INTRODUCTION

Surface wave sustained discharges (SWDs) generated in dielectric tubes are a special kind of HF (High Frequency) discharges with interesting features such a great flexibility, stability and reproducibility, or a wide range of operating conditions under which they can operate (broad range of frequencies, different support gases, different pressure conditions). These properties explain the increasing use of these discharges in applications such as elemental analysis,[1-3] surface treatment,[4,5] lighting,[6] destruction of contaminant gases,[7] or sterilization,[8] among other applications, and are responsible for the attention that these plasmas have attracted in the last decades. For surface treatment, SWDs generated at 2.45 GHz are very promising plasmas, since this frequency condition has shown to be convenient in applications such as Plasma Enhanced Chemical Vapour Deposition for thin films deposition or Plasma Etching, because the use of HF plasmas improves deposition and etching rates.[9,10] SWDs at low pressures provided successful results in applications of this kind,[11-13] but in the last years, the interest in studying SWDs at atmospheric pressure has grown significantly. This pressure condition simplifies the handling of SWDs, avoiding the use of complicated vacuum systems. Selwyn et al.[14] have claimed that, in addition to reduction in the capital cost of equipment and the elimination of constraints imposed by vacuum-compatibility, plasma processing at atmospheric pressure provides clear advantages over traditional vacuum-based plasma processing, offering improvements for generation of active chemical species, high chemical selectivity, minimal ion densities resulting in low surface damage, and surface treatment methods unachievable by other means.

In the last fifteen years, argon SWDs at atmospheric pressures have been widely studied,[15-20] as this gas is easy to ionize compared with other inert gases (such as neon and helium) and it is relatively cheap (more than xenon or krypton). They can be sustained using very small power levels (> 50 W) and in their generation no cooling device is needed to avoid

the tube damage because of their relatively low gas temperatures (~1200 K). In contrast, argon SWDs at atmospheric pressure are radially contracted and their volume is reduced.[21-22] These drawbacks limit their applications. Recent works have proved that it is possible to expand the argon plasma flame created at the end of a SWD column by making a helium gas flow around it.[23-24] Thus, the presence of helium around the flame provokes a plasma expansion because of the higher thermal conductivity of this gas, in such a way that the non-uniform gas heating along the discharge radius (typical of argon 2.45 GHz plasmas at atmospheric pressure) is reduced. Expanded plasma flames of different geometries and sizes can be obtained by varying argon and helium gas flow rates. The cooling with helium diminishes the electron temperature in the expanded plasma region from 7000 to 4000 K and the electron density from 4×10^{20} m^{-3} to 7×10^{19} m^{-3}.[24] The gas temperature in these flames is about 1200 K, notably inferior to those corresponding to the non-cooled (with helium) plasma flame (1800 K). Thus, this new configuration extends the possibilities of using argon SWDs at atmospheric pressure for surface treatment applications in which substrate damages provoked by ion bombardment or high gas temperatures might be avoided.

The purpose of the present work is to examine the excitation capability of this expanded plasma flame. The aim is to gain a basic insight into some reactive species and their excitation processes in this kind of HF plasma at atmospheric pressure. For this purpose, gases of different compositions (argon with different proportions of nitrogen) were introduced at the end of the expanded flame where plasma temperatures and population densities of some atomic argon levels were still high enough. Optical Emission Spectroscopy (OES) techniques were used to detect and identify the active species in the different plasma regions.

2. EXPERIMENTAL SET-UP

2.1. Plasma generation

Figure 1 shows the experimental set-up used for the creation of the plasma. A *surfaguide* device[25] was used to couple the energy coming from a microwave (2.45 GHz) generator (GMP 12 kT / t SAIREM) to the support gas (argon with a purity of 99.99 %) within a quartz tube of 1.5-4 mm of inner and outer diameter, respectively. In this work the microwave power was set at 240 W level and the length of the tube (3.3 cm from the coupler gap) was adjusted to achieve a plasma flame at its end. The electromagnetic field that sustained the complete discharge (previous *column* and *flame*) was provided by a travelling surface wave linked to the plasma-dielectric interface. This surface wave transmitted energy as it propagated throughout the discharge. This energy was partially employed to excite, to ionize and/or to dissociate the different species and molecules existing in the support gas. The movable plunger and stubs permitted the impedance matching in order to achieve the best energy coupling, so that the power reflected back to the generator (P_r) was negligible (< 5%).

The radial contraction phenomenon was responsible for the progressive constriction observed at both the end of the plasma column and the subsequent plasma flame. As shown in a previous work,[24] the external cooling of this plasma flame with helium reduced plasma contraction (radially and axially) and gave rise to an expanded flame. With this purpose, an external concentric tube (of 6-8 mm of inner and outer diameter, respectively) was employed to allow a helium gas (with a purity of 99.99 %) to flow around the discharge tube and the plasma flame. The length of the external tube was set long enough to avoid the contact plasma-air and reduce the air entrance into the plasma flame.

Argon and helium flow rates were set at 0.560 slm (standard litres per minute) and 0.340 slm levels, respectively, and an expanded flame of about 3.9 cm length was obtained (see Fig. 2). Argon (0, 100 and 200 sccm (standard cubic centimetres per minute)) with different

amounts (0, 50 and 100 sccm) of nitrogen (of 99.99 % purity) were introduced at the end part of the plasma flame from a side entrance of the external tube, as shown in Fig.2. Gas flow rates were controlled by means of HI-TEC (IB31) mass flow controllers.

Axial dimensions of these expanded flames are shown in Table I. In the present study, three different plasma regions were considered: *plasma column*, *expanded flame* and *end part* of the flame where the introduction of other gases was performed (for exciting them).

2.2. Optical Emission Spectroscopy

Figure 1 includes a scheme of the optical detection assembly and data acquisition system to process spectroscopic measurements. Light emission from the plasma was analyzed by utilising a Jobin-Yvon Horiba 1000M spectrometer (Czerny-Turner type) with 1 m of focal distance, a holographic diffraction grating of 2400 grooves/mm, and a typical spectral dispersion of 0.4 nm/mm in the visible range. The emission spectra were recorded employing a cooled CCD camera (Horiba Jobin Yvon) and slit widths of 100 μm. The light was side-on collected at each axial position of the plasma through an optical fibber (UV-VIS high OH fibber with a range of transmission wavelength 200-800 nm). A UV-VIS collimating beam probe was coupled to the optical fibber giving a 0º-45º of field of view and 3 mm of aperture. Thus, an Abel inversion was precluded and the radial study of the plasma could not be performed. Consequently, the values reported for the quantities measured in this work should be considered to be average ones for a transversal section of the plasma associated with a specific axial position. The axial origin of the measurements was located at the beginning of the plasma (y-axis). The flame started at the y = 3.3 cm position (end of the quartz tube) and introduction of argon/nitrogen took place at y = 6.5 cm position (see Fig. 2). Intensity measurements were calibrated by using a calibrated ribbon lamp with a known emission spectrum.[26]

3. RESULTS AND DISCUSSION

Spectra emitted at different axial positions of the whole SWD were recorded in the wavelength range from 220 to 730 nm. Figures 3 (a) and (b) show typical visible emission spectra corresponding to plasma column and expanded flame, respectively.

An exhaustive analysis of the different visible spectra emitted by the plasma at every axial position was performed in order to gain an insight into the processes governing the excitation kinetics in the different plasma regions. Special attention was paid to what occurred at the end part of the plasma when other gases (pure argon and argon containing nitrogen) were introduced, with the aim of knowing the excitation capability of this expanded flame.

The introduction of a gas at the end part originated a change in the shape of the flame at this region, intensifying the contact between the plasma and the tube wall. Moreover, when the gas introduced contained nitrogen (reactive gas), the introduction provoked a change in the colour of this plasma region (a pink colour was observed) and a decrease of the plasma (axial and radial) dimensions (see Table I), being the dominant features in the spectra due to species containing nitrogen.

Tables II and III summarize the emission lines and bands, respectively, identified in the experiments performed. As found by García *et al.* in a previous work,[24] atomic helium lines were not detected in any case, what indicated that helium atoms excitation in the expanded flame was not efficient enough to allow the detection of helium lines. This result is coherent with those presented by Muñoz and Calzada,[27] corresponding to the study of an argon-helium SWD column sustained at atmospheric pressure created at very high HF power levels (up to 2000 W). The lack of emission of ionic and atomic helium lines in the spectra is due to the high excitation energy of excited (and metastable) helium levels, and the high ionization potential of this gas.

Now a detailed presentation of the behaviour of the different excited species detected from OES is given.

3.1. Emission of first negative system of molecular ion $N_2^+(B^2\Sigma_u^+ \rightarrow X^2\Sigma_g^+)$

Figure 4 shows the axial behaviour along the plasma of the band head of first negative system of molecular ion N_2^+ ($B^2\Sigma_u^+ \rightarrow X^2\Sigma_g^+$) at 391.44 nm.

In the *column region* the existence of a small amount of molecular ions N_2^+ was detected. As in the case of other HF (2.45 GHz) plasmas at atmospheric pressure with similar electron density and temperature values, the presence of molecular ions N_2^+ can be ascribed to *charge transfer* reactions between argon ions and nitrogen molecules in their ground state, present as impurities in the main gas (coming from the entry of air into the plasma): [28]

$$Ar^+ + N_2\ (X^1\Sigma_g^+) \rightarrow Ar^0 + N_2^+\ (X^2\ \Sigma_g^+) \qquad (1)$$

This transfer is quasi-resonant because of the similar ionization energies for argon and molecular nitrogen. Molecular ions in the ground state $X^2\Sigma_g^+$ (15.7 eV) from reaction (1), could be excited towards $B^2\ \Sigma_u^+$ (18.9 eV) state from electron collisions

$$N_2^+\ (X^2\Sigma_g^+) + e^-\ (3.2\ eV) \rightarrow N_2^+\ (B^2\ \Sigma_u^+) + e^- \qquad (2)$$

Radiative decay towards the ground state originated the observed spectrum of first negative system of molecular ion N_2^+

$$N_2^+\ (B^2\Sigma_u^+) \rightarrow N_2^+\ (X^2\Sigma_g^+) + h\nu \qquad (3)$$

In the region of the *expanded flame*, the intensity of the N_2^+ first negative system grew up to position y = 5 cm, which could be ascribed to the higher amount of air impurities existing in this region (note that here the plasma occupied a larger extension and new air impurities were carried by helium gas). The subsequent intensity decrease observed can be explained taking into account that the density of argon ions taking part in reaction (1) progressively decayed along this plasma flame,[24] what also made the amount of N_2^+ species formed from them decrease. Moreover, electron energy and density were lower at the positions farther from coupling device, getting reaction (2) less effective.

At the *end part* of the flame, when pure argon was introduced, emission of N_2^+ first negative system extended until regions farther from coupling device (see Fig. 4). This seems to indicate that reactions (1) and (2) were still occurring in this plasma zone. On the other hand, the introduction of argon/nitrogen mixtures provoked a reduction of the emission of N_2^+ first negative system (see Fig. 4). In argon HF (2.45 GHz) torches sustained at atmospheric pressure, *dissociative recombination* reactions have been considered as possible channel for molecular nitrogen ions destruction[28,29]

$$N_2^+ + e^- \rightarrow N + N \qquad (4)$$

The presence of NH ($A^3\Pi \rightarrow X^3\Sigma^-$) and CN ($B^2\Sigma \rightarrow X^2\Sigma$) systems in the emission spectra of those plasmas proved[28-30] that dissociative recombination type reactions (4) were really occurring in the plasma even though nitrogen atomic lines had not been detected. In the argon HF plasma studied in the present work, NH ($A^3\Pi \rightarrow X^3\Sigma^-$) and CN ($B^2\Sigma \rightarrow X^2\Sigma$) bands were detected in the three zones considered (see Fig. 5). According to that, reactions (4) can be considered the mechanism controlling the loss of molecular nitrogen ions along all the plasma (column and expanded flame). Upon introduction of argon/nitrogen mixtures, the reduction of

the emission of N_2^+ observed at the end part of the expanded flame, together with the increase of the NH ($A^3\Pi \rightarrow X^3\Sigma^-$) emission detected in this zone, indicates that in this plasma region the dissociative recombination of nitrogen ions is enhanced by the nitrogen addition to the plasma.

3.2. Emission of second positive system of N_2 ($C^3\Pi_u \rightarrow B^3\ \Pi_g$)

Figure 6 depicts the axial behaviour along the plasma of the N_2 second positive system ($C^3\Pi_u \rightarrow B^3\ \Pi_g$) band head at 357.6 nm.

The presence of N_2 ($C^3\Pi_u$) states in both plasma column and expanded flame can be ascribed to excitation transfer from argon metastables (E ~ 11.5 – 11.8 eV) towards ground state of molecular nitrogen (E ~ 11.1 eV)[28,29,31,32]

$$Ar^m + N_2\ (X^1\Sigma_g^+) \rightarrow Ar^0 + N_2\ (C^3\Pi_u) \qquad (5)$$

Emissions from N_2 ($C_3\Pi_u$) are enhanced by reaction (5) which results in an enhancement of the emission of N_2 second positive system

$$N_2\ (C^3\Pi_u) \rightarrow N_2\ (B^3\Pi_g) + h\nu \qquad (6)$$

The increase of emission of N_2 second positive system in the expanded flame until y = 4 cm position can be again attributed to the entrance of a higher amount of air impurities in this plasma region.

In the end part of the expanded flame, pure argon introduction provoked that the emission of N_2 second positive extended until regions farther from surfaguide. The introduction of argon containing nitrogen originated a remarkable increase of N_2 second

positive emission, which exhibited a maximum at y = 7 cm position (see Fig. 6). These results suggest that reaction (5) continues taking place in this plasma zone where argon metastable atoms are the main energy carriers to generate reactive species N_2. Certainly, in this region where electron temperature and density are relatively low, it could be expected that electron collisions do not play an important role in the excitation process of plasma species, being the excitation mechanism of N_2 molecules mainly controlled by excitation reactions with argon metastables.

On the other hand, it is important to realise that argon metastables would not have energy enough to create new N_2^+ ($B^2\ \Sigma_u^+$) states (18.9 eV) from the following Penning type reactions like[29]

$$A^m + N_2\ (X^1\Sigma_g^+) \rightarrow A^0 + N_2^+\ (B^2\ \Sigma_u^+) + e^- \qquad (7)$$

which is coherent with the results obtained in the precedent section. Moreover, the small changes in N_2^+ first negative observed also indicate that helium metastable atoms (E ~ 19.8 eV), which could be able to induce reaction (7), must not be present in this plasma region.

3.3. Emission of argon atomic lines

Table II shows some argon atomic (Ar I) lines detected in the plasma column and the expanded flame. The emission of these lines axially diminished as the distance to the coupling device increased, what indicated that the population density of the corresponding upper levels from which radiative transitions took place also decreased, as typical in argon SWDs.[15,16] Figure 7 depicts the axial evolution of the intensity of 714.7 nm argon line throughout all the plasma, evolution that was similar to those exhibited by the rest of Ar I lines detected.

García *et al.*[16] have explained that in argon SWDs columns at atmospheric pressure (where electron density is still high enough) the axial behaviour of the population density of argon atomic excited levels *5p* and higher ones is determined by the electron and argon atomic ions densities, being ruled by electron controlled *Saha balances*. On the other hand, Sainz et al.[20] have shown that argon molecular ions Ar_2^+ in argon SWD columns at atmospheric pressure also play an outstanding role in the plasma excitation kinetics. For the expanded flame studied in the present work, it has not been still established what kind of kinetic processes controls the population of argon excited levels. Even though preliminary studies performed[24] seem to indicate that atomic ion-electron three body recombination

$$Ar^+ + e^- + e^- \rightarrow Ar^{**} + e^- \qquad (8)$$

could continue playing an important role in the formation of high excited states of argon, molecular ion-electron dissociative recombination

$$Ar_2^+ + e^- \rightarrow Ar^{**} + Ar^0 \qquad (9)$$

should not be discarded.

In the end part of the expanded flame, Ar^+ and Ar_2^+ species would be likely created by pooling Penning ionization reactions from argon metastable atoms: metastable-metastable ionization collisions and metastable-metastable associative ionization, respectively.[20,33]

Upon pure argon introduction in the end part of expanded flame, emission of the lines of the Ar I system lightly extended until positions farther from coupling device, as a consequence of the existence of a higher amount of argon. So, at this discharge position, the

plasma still has capability to create new atomic argon species when argon is added from the outside.

On the other hand, when argon containing nitrogen was added, a sharply decrease of the intensity of all Ar I lines detected was observed, only the strongest argon lines (corresponding to *4p - 4s* radiative transitions, producing metastable atoms) remaining visible. Therefore, all activated argon species were quenched, showing a similar decreasing tendency as when nitrogen flow rate was raised. These results indicate that argon excited atoms were consumed by the nitrogen addition. The almost entire quenching of atomic argon levels can be understood by considering the results commented previously in Sections 3.1 and 3.2. Firstly, nitrogen addition originates a depopulation of argon metastable levels (argon metastable atoms transfer their energy to gas reactive species N_2 from reactions of excitation transfer type (5)), what affects the processes of creation of ions Ar^+ and Ar_2^+, and consequently, the argon excitation processes described by reactions (8) and (9).[33] Furthermore, nitrogen addition causes a reduction of argon ions from charge transfer type reactions (1), what also diminishes the formation of highly excited argon neutral states from three-body recombination of argon ions.

3.4. Emission of hydrogen atomic lines and NH $(A^3\Pi \rightarrow X^3\Sigma^-)$ and CN $(B^2\Sigma \rightarrow X^2\Sigma)$ systems

The emission of the hydrogen atomic lines H_α and H_β was detected at different plasma positions. Hydrogen atoms were present in the discharge as impurities in the carrier gas.

As shown in Fig. 8, the intensity of the hydrogen lines decreased along the plasma column (typical behaviour in argon SWDs[16]) and experimented a light increase at y = 5 cm position in the expanded plasma flame due to the greater amount of hydrogen atoms existing in this zone, carried by argon and helium main gases. At the end part of the plasma flame,

again the intensity of these lines went sharply down when argon containing nitrogen was added.

As commented previously, the presence of NH ($A^3\Pi \rightarrow X^3\Sigma^-$) and CN ($B^2\Sigma \rightarrow X^2\Sigma$) systems in the emission spectra demonstrated that dissociative recombination type reactions (4) were occurring in the plasma. Thus, molecular species NH and CN were likely created by three body association type reactions

$$A + N + S \rightarrow AN^* + S \qquad (10)$$

where A (H or C) and N were associated in the presence of a spectator, S. The formation of NH molecules via reaction (10) could be an important channel of hydrogen level depopulation at the end of the expanded flame when argon containing nitrogen is introduced. This hypothesis seems to be confirmed by the results observed in Figure 5: the addition of argon/nitrogen provoked an increase of the NH band head intensity, that is, the formation of NH molecules just when population of H I levels decayed.

3.5. Emission of sodium atomic lines

In the expanded flame zone, due to the plasma expansion towards the walls of the external tube, some wall etching took place and new lines corresponding to quartz impurities were detected.

In this way, two very intense lines appeared at 588.99 and 589.59 nm corresponding to resonant transitions from *3p* states of Na I system (of very low excitation energy, 2.1 eV) towards ground state. These lines were especially intense at y = 4 cm axial position of the expanded flame where the contact plasma-wall was maximum (see Fig. 9).

In the plasma column, emission of these lines was no detected because of the radial contraction of argon column.

When pure argon was introduced in the end part of the expanded flame, the emission of these lines was outstandingly enhanced at y = 7 cm axial position (see Fig. 9). Certainly, this kind of side introduction of the gas, provoked a deformation of the shape of the end part of the plasma, increasing the contact plasma-wall, which resulted in a higher amount of sodium atoms present in this plasma region. Just by looking at this region, a strong yellow emission (corresponding to these two intense Na I lines) was observed.

Figure 9 also shows how the emission of these lines was even more enhanced when nitrogen was added together with the argon. Ricard *et al.*[34] have also observed atomic lines of sodium in argon-nitrogen post discharges. The emission of these lines comes from atomic levels that are in resonance with the vibrational levels of N_2 ($X^1\Sigma_g^+$) state, and therefore, are populated from reactions

$$N_2\ (X^1\Sigma_g^+,\ v) + Na^0 \Rightarrow N_2(X^1\Sigma_g^+,\ v') + Na^* \qquad (11)$$

From the results obtained in the present work, it can be deduced that similar reactions seems to be occurring in the argon SWD expanded flame studied.

3.6. Emission of OH ($A^2\Sigma^+ \rightarrow X^2\Pi$) system

Figure 10 shows the axial behaviour of the band head of OH ($A^2\Sigma^+ \rightarrow X^2\Pi$) ro-vibrational band at 308.90 nm along the plasma. The presence of radical OH in the plasma is due to the existence of impurities coming from the etching of the tube walls. In the region of the column where argon plasma is radially contracted, the intensity of this band was small. In the region of the expanded flame, near y = 4 cm axial position, where a better plasma-wall contact

existed, emission of OH band head reached a very high value. Finally, at the end part of the flame, when argon/nitrogen gas was added, emission of OH increased again because the plasma-wall contact was intensified in this zone.

4. CONCLUSIONS

The excitation capability of an argon SWD expanded plasma flame at atmospheric pressure has been studied, by using Optical Emission Spectroscopic techniques in order to gain a basic insight into some reactive species and their excitation processes in this kind of HF plasma at atmospheric pressure. In this way, gases of different compositions (argon with different proportions of nitrogen) have been introduced at the end region of the expanded flame where plasma temperatures and the population densities of atomic argon levels were still high enough.

The introduction of *pure argon* in this plasma flame provoked a moderate raise of the emission intensities of atomic argon spectral lines and NH, CN, N_2 (coming from air impurities in the main gases, argon and helium) ro-vibrational band heads, in this final plasma zone. This fact shows that, at this point, the plasma continues having excitation capacity of new argon and other species, coming from the outside.

When *argon containing nitrogen* was added to the end part of the plasma flame:

1) All atomic argon lines emitted in this plasma region were highly quenched, with only the strongest argon lines remaining visible (corresponding to *4p - 4s* transitions);

2) A noticeable increase in the emission of N_2 second positive system ($C^3\Pi_u - B^3\Pi_g$) was observed in this plasma zone;

3) On the contrary, the weak emission of N_2^+ first negative system ($B^2\sum_u^+ - X^2\sum_g^+$) was only lightly affected, and

4) Finally, the emission of 588.99 nm and 589.59 nm spectral lines corresponding to Na I system was strongly enhanced.

As reactive gases were added at the end part of the expanded plasma flame where the electron temperature and density were low, it could be expected that electron collisions do not play an important role in their excitation process. So in this plasma region, the excitation process of N_2 molecules could be likely ruled by reactions of excitation transfer from argon metastables atoms towards the ground state of molecular nitrogen. Thus, metastable argon atoms from the expanded flame would be the main energy carriers to generate reactive species in this plasma zone: the metastable argon atoms (E ~11.5–11.8 eV) have energy high enough to excite state N_2 ($C^3\Pi_u$) second positive (E ~11.1 eV). On the contrary, argon metastable atoms have not sufficient energy to generate $N_2^+(B_2\ \Sigma_u^+)$ states (E ~18.7eV) from Penning type reactions (7), which is coherent with the behaviour N_2^+ first negative band head observed.

The small decrease in N_2^+ first negative observed upon argon/nitrogen introduction, indicates that dissociative recombination reactions (4) are enhanced and helium metastable atoms (E ~ 19.8 eV), which could be able to induce reactions (7) and so raise the density of N_2^+ species, must not be present in this plasma region.

As the plasma expanded to the walls of the external tube, some plasma etching of its inner wall took place, and some new lines corresponding to impurities in the quartz were observed in the expanded flame spectra. In this way, two very intense lines appeared at 588.99 nm and 589.59 nm, corresponding to transitions from *3p* Na I levels (of very low excitation energy 2.10 eV) to the atomic ground state.

In the zone of side introduction of pure argon or argon/nitrogen gases, the emission of these sodium lines was especially intense. Certainly, this kind of introduction provoked a

deformation of the shape of the plasma end part, increasing the contact plasma-tube wall, which resulted in a more effective etching of the inner wall of the external tube.

The emission of the sodium lines became still more intense when nitrogen was added together with the argon. This enhancement is related to the resonant energy transfer from vibrational levels of N_2 ($X^1\Sigma_g^+$) state towards Na I levels.

ACKNOWLEDGMENTS

The authors are grateful to Adolfo García for his help during the preparation of the manuscript. We are also indebted to André Ricard for very interesting discussions.The authors are also grateful to *Espectroscopía de Plasmas* research group for its technical support. This work has been partially subsidised by the Ministry of Science and Technology (Spain) in the framework of the project no. ENE2005-00314 and the European Community (FEDER) Founds.

REFERENCES

1. J. Hubert, M. Moisan and R. Ricard, Spectrochim. Acta B **33**, 1 (1979).

2. M. Selby, R. Rezaaaiyaan and G.M. Hieftje, Appl. Spectrosc. **41**, 749 (1987).

3. J. Hubert, S. Bordeleau, K.C. Tran, S. Michaud, B. Milette, R. Sing, J. Jalbert, D. Boudreau, M. Moisan and J. Margot, Fresenious J. Anal. Chem. **355**, 494 (1996).

4. S. Shelz, C. Campillo and M. Moisan, Diamond and Relat. Mater. **7**, 1675 (1998).

5. S. Ilías, C. Campillo, C.F.M.Borges and M. Moisan, Diamond and Relat. Mater. **9**, 1120 (2000).

6. D. Baeuchemin, J. Hubert and M. Moisan, Appl. Spectrosc. **40**, 379 (1986).

7. Y. Kabouzi, M. Moisan, J.C.Rostaing, C. Trassy, D. Guerin, D. Keroack and Z. Zakrzewski J. Appl. Phys. **93**, 9483 (2003).

8. S. Moreau, M. Moisan, M. Tabrizian, J. Barbeau, J. Pelletier, A. Ricard and L. Yahia *J.* Appl. Phys. **88**, 1166 (2000).

9. M.R. Wertheimer, M. Moisan, J.E. Klemberg-Sapieha and R. Claude, Pure & Appl. Chem **60**, 815 (1988).

10. M.R. Wertheimer and M. Moisan, J.Vac. Sci. Technol. **3**, 2643 (1985).

11. M. Moisan and M.R. Wertheimer, Surf. Coat. Techn. **59**, 1 (1993).

12. L. Paquin, D. Masson, M.R. Wertheimer and M. Moisan, Can. J. Phys. **63**, 831 (1985).

13. A. Barranco, J. Cotrino, F. Yubero, J.P. Espinós, J. Benítez, C. Clero and A.R. González-Elipe, Thin Solid Films **401**, 150 (2001).

14. G.S. Selwyn, H.W. Herrmann, J. Park, and I. Henins. Contrib. Plasma Phys. **6**, 610 (2001).

15. M.D. Calzada, M. Moisan, A. Gamero, and A. Sola J. Appl. Phys. **80**, 46 (1996).

16. M.C. García, A. Rodero, A. Sola and A. Gamero, Spectrochim. Acta B **55**, 1733 (2000).

17. M.C. García, A. Rodero, A. Sola and A. Gamero, Spectrochim. Acta B **55**, 1611 (2000).

18. M.C. García, A. Rodero, A. Sola and A. Gamero, Spectrochim. Acta B **57**, 1727 (2002).

19. M.D. Calzada, M. Sáez and M.C. García, J. Appl. Phys. **88**, 34 (2000).

20. A. Sáinz, J. Margot, M.C. García and M.D. Calzada, J. Appl. Phys. **97**, 113305 (2005).

21. Y. Kabouzi, M.D. Calzada, M. Moisan, K.C. Tran and C. Trassy, J. Appl. Phys. **91**, 1008 (2002).

22. E. Castaños-Martínez, Y. Kabouzi, K. Makasheva and M. Moisan, Phys. Rev. E **70**, 066405 (2004).

23. M.C. García, C. Yubero, M. Varo and P. Martínez, CIP 07 Abstracts Booklet, 107 (2007).

24. M.C. García, M. Varo and P. Martínez, Appl. Spectros. **63**, 822 (2009).

25. C.M. Ferreira and M. Moisan, *Microwave discharges: Fundamentals and Applications*, (NATO ASI Series B, Plenum, New York, 1993), Vol. 302.

26. C. Yubero, M.C. García and M.D. Calzada, Optica Applicata **38**, 353 (2008).

27. J. Muñoz and M.D. Calzada, J.Phys.D: Appl. Phys. **41**, 135203 (2008).

28. E.A.H. Timmermans, J. Jonkers, I.A.J. Thomas, A. Rodero, M.C. Quintero, A. Sola, A. Gamero and J.A.M. van der Mullen, Spectrochim. Acta B **53**, 1553 (1998).

29. G. P. Jackson and F.L. King, Spectrochim. Acta B **58**, 185 (2003).

30. M.C. García, C. Yubero, M.D. Calzada and M.P. Martínez-Jiménez, Appl. Spectros. **59**, 519 (2005).

31. Q.S. Yu and H.K. Yasuda, Plasma Chem. and Plasma Process. **18**, 461 (1998).

32. N. Britun, M. Gaillard, A. Ricard, Y.M. Kim, K.S. Kim and H.G. Han, J. Phys. D: Appl. Phys. **40**, 1022 (2007).

33. N. Kang, N. Britum, S. Oh, F. Gaboriau and A. Ricard, J. Phys. D: Appl. Phys. **42**, 112001 (2009).

34. A. Ricard, T. Czerwiec, T. Belmonte, S. Bockel and H. Michel, Thin Solid Films **341**, 1 (1999).

FIGURE CAPTIONS

Figure 1. Block diagram of the experimental setup used.

Figure 2. Details of the *plasma column*, *expanded torch* and zone of introduction of external gases.

Figure 3. Typical optical spectra emitted by (a) plasma column and (b) expanded flame.

Figure 4. Intensities of the band head of N_2^+ ($B^2\Sigma_u^+ \rightarrow X^2\Sigma_g^+$) at 391.44 nm, emitted by the plasma at different axial positions when different proportions of Ar/N_2 were introduced (F_{Ar} = 200 sccm).

Figure 5. Intensities of the band head of NH ($A^3\Pi \rightarrow X^3\Sigma^-$) at 336.01 nm, emitted by the plasma at different axial positions when different proportions of Ar/N_2 were introduced (F_{Ar} = 200 sccm).

Figure 6. Intensities of the band head of N_2 ($C^3\Pi_u \rightarrow B^3\ \Pi_g$) at 357.6 nm, emitted by the plasma at different axial positions when different proportions of Ar/N_2 were introduced (F_{Ar} = 200 sccm).

Figure 7. Intensities of 714.7 line of Ar I system as a function of axial position measured when different proportions of Ar/N_2 were introduced (F_{Ar} = 200 sccm).

Figure 8. Intensities of H_α line of H I system as a function of axial position measured when different proportions of Ar/N_2 were introduced (F_{Ar} = 200 sccm).

Figure 9. Intensities of 589.59 line of Na I system as a function of axial position measured when different proportions of Ar/N_2 were introduced (F_{Ar} = 200 sccm).

Figure 10. Intensities of the band head of OH ($A^2\Sigma^+ \rightarrow X^2\Pi$) at 308.90 nm, emitted by the plasma at different axial positions when different proportions of Ar/N_2 were introduced (F_{Ar} = 200 sccm).

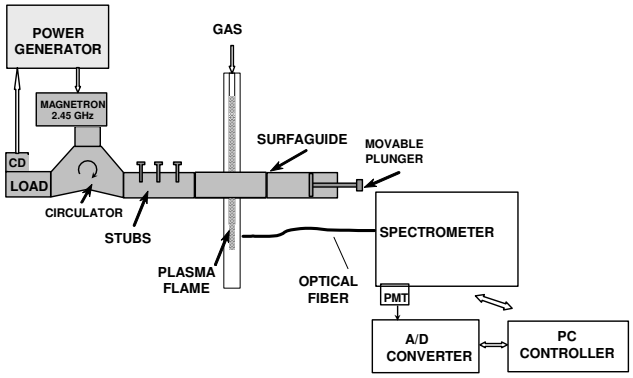

Fig. 1. García et al.

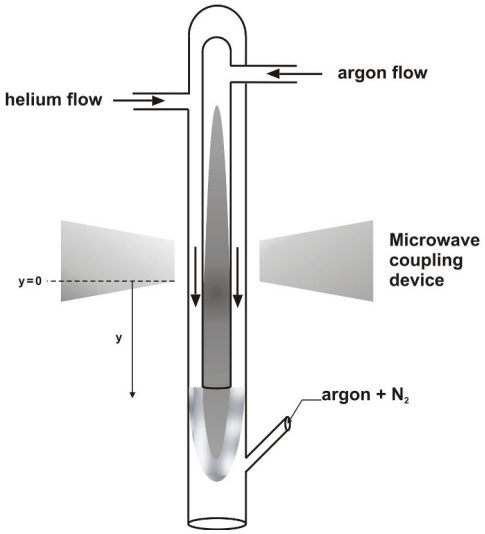

Fig. 2. García et al.

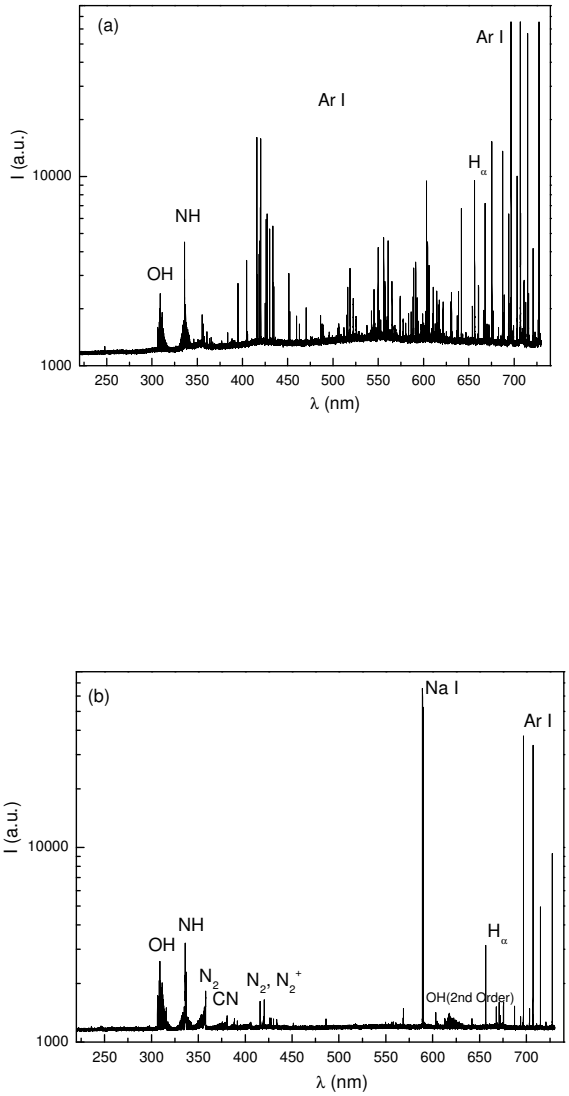

Fig. 3. García et al.

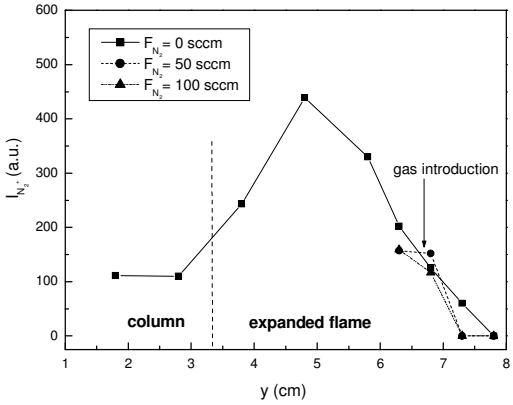

Fig. 4. García et al.

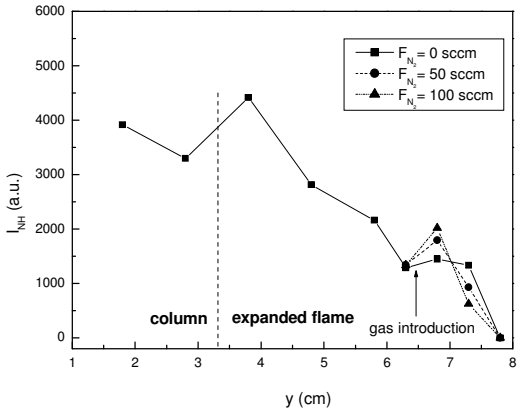

Fig. 5. García et al.

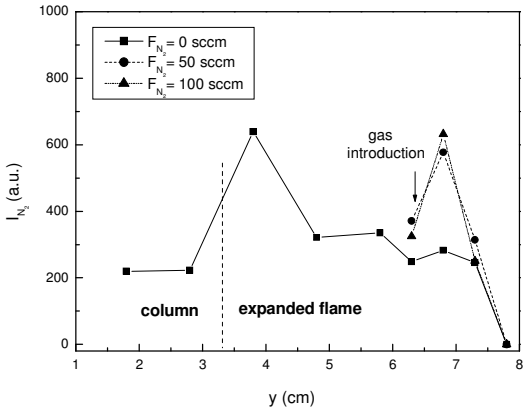

Fig. 6. García et al.

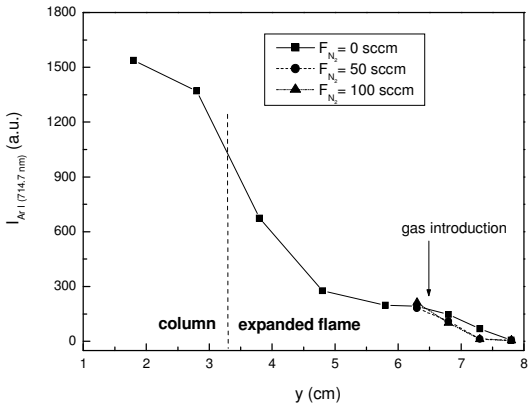

Fig. 7. García et al.

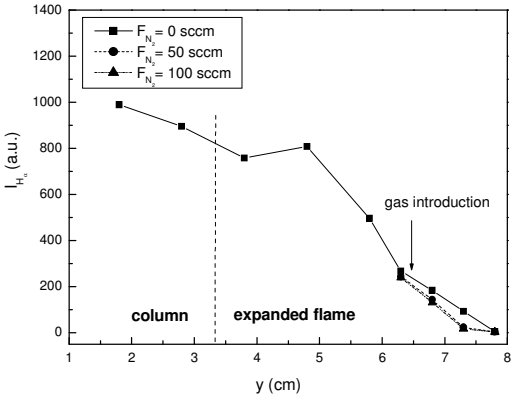

Fig. 8. García et al.

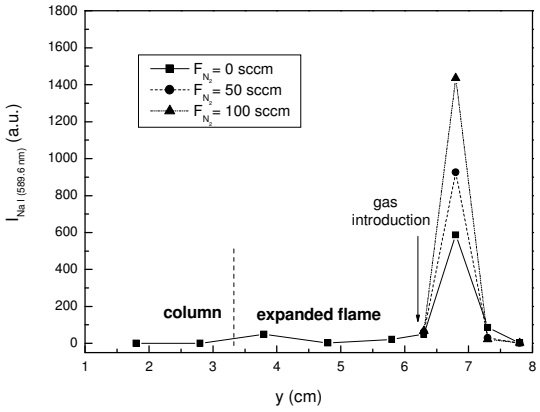

Fig. 9. García et al.

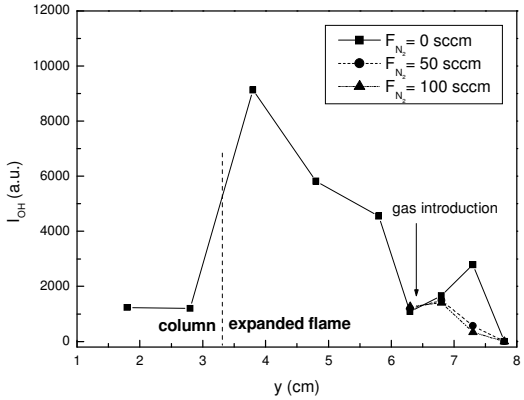

Fig. 10. García et al.

Table I. Axial dimensions of the expanded plasma flame when different proportions of Ar/N_2 were introduced at its end region.

	F (N_2) = 0 sccm	F (N_2) = 50 sccm	F (N_2) = 100 sccm
F (Ar) = 0 sccm	3.9 cm	3.4 cm	3.4 cm
F (Ar) = 100 sccm	4.0 cm	3.5 cm	3.5 cm
F (Ar) = 200 sccm	4.0 cm	3.5 cm	3.5 cm

Table II. Atomic emission lines detected in the plasma (column and expanded flame).

Species	λ (nm)	E_p (eV)	Transition
Ar I	714.70	13.28	4p' - 4s[*]
	706.72	13.30	4p' - 4s[*]
	727.29	13.32	4p' - 4s
	696.54	13.32	4p' - 4s[*]
	425.12	14.46	5p - 4s[*]
	430.01	14.50	5p - 4s
	427.22	14.52	5p - 4s
	426.63	14.52	5p - 4s
	434.52	14.68	5p' - 4s'
	433.53	14.68	5p' - 4s'
	433.36	14.68	5p' - 4s'
	425.93	14.73	5p'-4s'
	675.28	14.74	4d - 4p
	641.63	14.83	6s - 4p
	591.21	15.00	4d'- 4p
	565.07	15.10	5d - 4p
	560.67	15.11	5d - 4p
	603.21	15.13	5d – 4p
	555.87	15.13	5d - 4p
	518.77	15.29	5d' - 4p
	549.58	15.33	6d - 4p
	522.12	15.44	7d - 4p
Na I	588.99	2.10	3p – 3s
	589.59	2.10	3p – 3s
H I	486.13	12.74	4d – 2p
	656.28	12.08	3d – 2p

Table III. Emission bands detected in the plasma (column and expanded flame).

Species	λ (nm)	Transition	*v', v''*
OH	308.90	$A^2\Sigma^+ \rightarrow X^2\Pi$	0, 0
NH	336.01	$A^3\Pi \rightarrow X^3\Sigma^-$	0, 0
N_2	337.13	$C^3\Pi_u \rightarrow B^3\ \Pi_g$	0, 0
	353.67	$C^3\Pi_u \rightarrow B^3\ \Pi_g$	1, 2
	357.69	$C^3\Pi_u \rightarrow B^3\ \Pi_g$	0, 1
	380.49	$C^3\Pi_u \rightarrow B^3\ \Pi_g$	0, 2
CN	386.19	$B^2\Sigma \rightarrow X^2\Sigma$	2, 2
	387.14	$B^2\Sigma \rightarrow X^2\Sigma$	1, 1
	388.34	$B^2\Sigma \rightarrow X^2\Sigma$	0, 0
N_2^+	358.21	$B^2\Sigma_u^+ \rightarrow X^2\Sigma_g^+$	1, 0
	391.44	$B^2\Sigma_u^+ \rightarrow X^2\Sigma_g^+$	0, 0